

Modelling and system identification of an experimental apparatus for anomaly detection in mechanical systems [☆]

Amol M. Khatkhate, Asok Ray ^{*}, Eric Keller

Department of Mechanical Engineering, The Pennsylvania State University, University Park, PA 16802-1412, United States

Received 1 December 2004; received in revised form 1 November 2005; accepted 14 December 2005
Available online 20 February 2006

Abstract

This paper presents design, modelling and system identification of a laboratory test apparatus that has been constructed to experimentally validate the concepts of anomaly detection in complex mechanical systems. The test apparatus is designed to be complex in itself due to partially correlated interactions amongst its individual components and functional modules. The experiments are conducted on the test apparatus to represent operations of mechanical systems where both dynamic performance and structural durability are critical.

© 2005 Elsevier Inc. All rights reserved.

Keywords: Anomaly detection; System identification; Time series analysis; Fatigue crack damage; Robust control; Real time computation

1. Introduction

An anomaly is defined as deviation from the nominal behavior of a dynamical system and is often associated with parametric and non-parametric changes that may gradually evolve in time. Anomalies may manifest themselves with self excitation within the dynamical system, or under persistent excitation of exogenous stimuli. The anomalies may be benign or malignant depending on their impact on the mission objectives and operating conditions. Major catastrophic failures in complex engineering systems could often be averted if the malignant anomalies are detected at an early stage.

The goal of the detection method [1] is to make inferences on occurrence of slow-time-scale anomalies (e.g., evolution of fatigue crack damage) in complex mechanical systems based on observed macroscopic changes in the behavior pattern of the *fast-time-scale* process dynamics. Since accurate and computationally tractable modelling of complex system dynamics is often infeasible solely based on the fundamental principles of

[☆] This work has been supported in part by Army Research Office (ARO) under Grant No. DAAD19-01-1-0646.

^{*} Corresponding author. Tel.: +1 814 8656377; fax: +1 814 8634848.

E-mail addresses: amk303@psu.edu (A.M. Khatkhate), axr2@psu.edu (A. Ray), EEK105@psu.edu (E. Keller).

physics, it is necessary to rely on time series data generated from sensors and other sources of information [2,3]. Along this line, Ray [1] has reported a novel concept of anomaly detection in complex systems, where the underlying information on the dynamical behavior is derived from time series data based on the following assumptions:

- The process has stationary dynamics at the fast time scale;
- Any observable non-stationary behavior is associated with changes evolving at the slow time scale at which anomalies may occur.

From the above perspectives, anomaly detection in dynamical systems [1] is formulated as a two-time-scale problem. Progression of anomalies may take place in the form of parametric or non-parametric variations in the system response and the objective is to capture this information from the observed time series data as early as possible. Thus, early detection of malignant anomalies allows a decision and control system to take appropriate actions, averts catastrophic failures, and possibly satisfies the mission requirements albeit at a degraded level of performance.

This paper focuses on design, modelling and system identification of an experimental test apparatus that has been recently fabricated for early detection of small anomalies. Critical parameters (e.g., resonant frequencies) of the test apparatus system provide meaningful information for detection of anomalies that accrue from fatigue crack damage in the mechanical structures. A mathematical model of the system dynamics is formulated for identification of these critical parameters from the input/output time series data generated by persistent excitation. (*Note:* Fatigue damage evolves at a time scale that is several orders of magnitude slower than the structural dynamics.)

The paper is organized in seven sections including the present one. Section 2 briefly describes the test apparatus for anomaly detection along with the design requirements for anomaly detection. Section 3 provides the details of systems modelling from physical aspects and determines the critical dimensions of the test apparatus and the expected resonant frequencies of the mechanical structure. Section 4 describes the frequency-domain identification approach and presents the pertinent results. Section 5 compares the identified model with experimental data. Section 6 discusses how the fatigue crack damage evolves as an anomaly in the dynamic behavior of the test apparatus and presents the results of anomaly detection. Section 7 concludes the paper and highlights the areas of future research.

2. Description of the test apparatus

With the goal of investigating decision and control strategies for damage reduction (i.e., to make the structural damage as small as possible) in complex mechanical systems (e.g., vehicular systems, power generation systems, and chemical plants), the test apparatus is designed to deliberately introduce fatigue damage in its critical component(s) [4]. These components are intentionally made to break in a reasonably short period of time to enhance the speed of conducting experiments. It is important that the damage in a critical component must not be strongly coupled with the plant dynamic performance. For example, a fatigue test machine, whose performance is directly related to the damage of the test specimens, does not qualify as such a test apparatus. From these perspectives, the requirements of the test apparatus are:

1. Operability under cyclic loading with multiple sources of input excitation;
2. Damage accumulation in test specimens (at selected locations) within a reasonable period of time with negligible damage in other components of the test apparatus;
3. Existence of moderate coupling between the damage of test apparatus and dynamic performance of the control system;
4. Accommodation of multiple failure sites for comparative evaluation of damage behavior and their trade-off and
5. Initiation of the groundwork for the implementation of a damage mitigating supervisory control system that makes decisions related to life extension without significant loss in performance [4].

Remark 1. The implication of Requirement #3 is as follows. The plant states that influence the structural damage in the test specimens should not strongly affect the performance variables under normal operating conditions. The rationale is that a strong coupling will preclude any application of life extending control to achieve a large gain in structural durability without any significant loss of performance. Nevertheless, moderate coupling is necessary because the analyzed time series data of the displacement sensor signal must contain ample information on the system dynamics. If this assumption is relaxed, early detection by mechanical sensors may not be feasible and one would have to rely entirely on damage sensing devices like ultrasonic transducers used in non-destructive testing for anomaly detection. The focus of this research is to show the efficacy of real-time anomaly detection based on time series data from mechanical sensors such as displacement sensors and accelerometers.

Remark 2. Small structural anomalies in critical components may not often affect the nominal plant dynamics and hence there is no inherent damage feedback. The rationale is that the physical phenomena of material degradation in plant component microstructures may not appreciably alter its macroscopic mechanical behavior (e.g., stiffness constant or natural modes of vibration) within the range of its normal service life. For example, fatigue-induced small cracks in an aircraft wing may not alter flight dynamics within its safe operating life span.

In order to satisfy the above requirements, the test apparatus is designed and fabricated as a three degree-of-freedom (DOF) mass beam structure that is excited by two shaker tables (i.e., vibrators). A schematic diagram of the test apparatus system is shown in Fig. 1 and dimensions of the pertinent components are listed in Table 1. The test apparatus system is logically partitioned into two subsystems: (i) the plant subsystem consisting of the mechanical structure including the test specimens to undergo fatigue crack damage; actuators and sensors and (ii) the instrumentation and control subsystem consisting of computers, data acquisition and processing, and communications hardware and software. The sensors include: two load cells for force measurement and two Linear Variable Displacement transducer (LVDT) for displacement measurement. Two of the three major DOF's are directly controlled by the two shaker table actuators, Shaker #1 and Shaker #2, and the remaining DOF is observable via displacement measurements of the three vibrating masses: Mass #1, Mass #2 and Mass #3. The inputs to the multi-variable mechanical structure are the forces exerted by the two shaker tables; and the outputs to be controlled are the displacements of Mass #2 and Mass #3.

The three beams in Fig. 1 are representatives of plant components, which are subjected to fatigue crack damage. The mechanical structure is excited at one or more of the resonant frequencies so that the critical component(s) can be subjected to different levels of cyclic stresses with no significant change in the external power injection into the actuators. The excitation force vector, generated by the two actuators, serves as

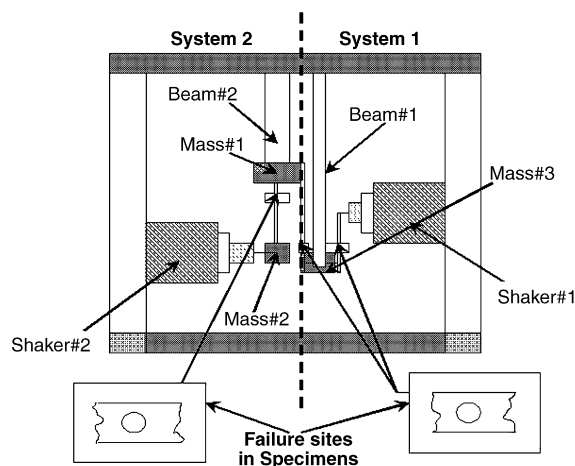


Fig. 1. Schematic diagram for the test apparatus.

Table 1
Structural dimensions of the test apparatus

Component	Material	Length (mm), mass (kg) (length × width × thickness)
Mass 1	Mild steel	1.0
Mass 2	Aluminium 6061-T6	0.615
Mass 3	Mild steel	2.2
Beam 1	Mild steel	800 × 25.4 × 12.7
Beam 2	Aluminium 6061-T6	711.2 × 22.2 × 11.1
Specimens	Aluminium 6061-T6	203.2 × 22.2 × 11.1

the inputs to the multi-DOF mechanical structure to satisfy the Requirement #1. The failure site in each specimen, attached to the respective mass is a circular hole (of radius 0.332 in. dia.) as shown in Fig. 1.

The three test specimens, each of which having a drilled hole as shown in Fig. 1, are excited at different levels of cyclic stresses. Notice that two of them are directly affected by the vibratory inputs while the remaining one is subjected to resulting stresses, thus functioning as a coupling between the two vibrating systems. In the present configuration, three test specimens are identically manufactured and their material is 6061-T6 aluminium alloy. In the future research, different materials will be selected for individual specimens that may also undergo different manufacturing procedures.

3. Modelling of the test apparatus system

A structural model of the mechanical system described above, is formulated using a cubic interpolation polynomial to approximate the lateral displacement of the beams and a linear approximation for the lateral displacement of the masses. The major assumptions in the model formulation include:

- Lumped representation of the beam masses.
- Beams are subjected to pure bending.

The first assumption implies that the beam masses essentially behave as rigid bodies, which is justified by their relatively high stiffness. The second assumption implies that deformation and rotation of the masses are negligible.

Since the objectives of the test apparatus also include investigation of different control policies and their influence on specific modes of fatigue failure in a dynamic setting, structurally weakened elements that are representatives of critical plant components, are introduced in the test apparatus to facilitate occurrence of observable failures. In the two-mass configuration of Fig. 1, three parallel failure sites are introduced by drilling a hole of diameter 0.332 in. in each of the beams connecting Mass #1 and Mass #2 and Mass #3 and vibrator #1. Fig. 2 shows the details of the failure site on the beam connecting Mass #1.

3.1. Subsystem modelling

Fig. 3 shows the local co-ordinate system for each component along with the sign convention used for forces and bending moments. Physics-based modelling of the system dynamics provides ample information

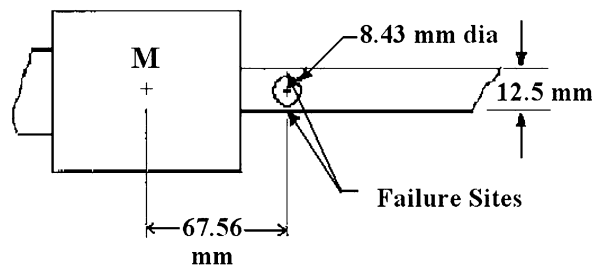


Fig. 2. Side view of failure site on the beam specimen.

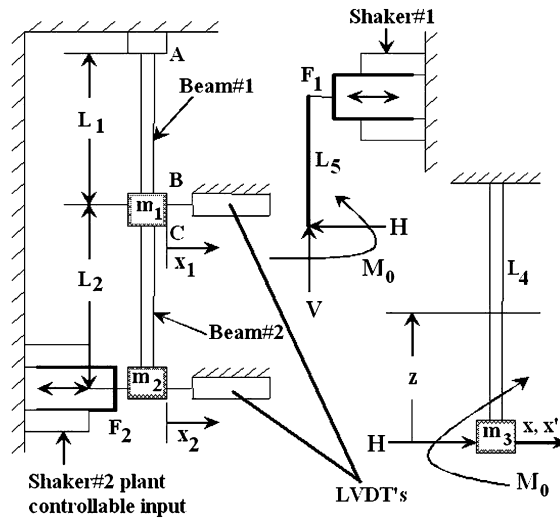


Fig. 3. Free body diagram.

on the resonant frequencies of the structure to estimate the appropriate dimensions for the various components. Furthermore, to cause fatigue failure within a reasonable amount of time, the specimens need to be subjected to loads near resonating conditions, as seen in Fig. 4.

The two subsystems 1 and 2 in Fig. 3 are connected by a thin aluminium beam and the failure site is designed as seen in Fig. 1. In the current configuration, all three specimens are identical and manufactured from the same process so as to facilitate comparative behavior under fatigue failure.

3.1.1. Analysis of System 1

The bending moment generated by Shaker 1 is

$$M_0 = F_1(L_5 - z). \tag{1}$$

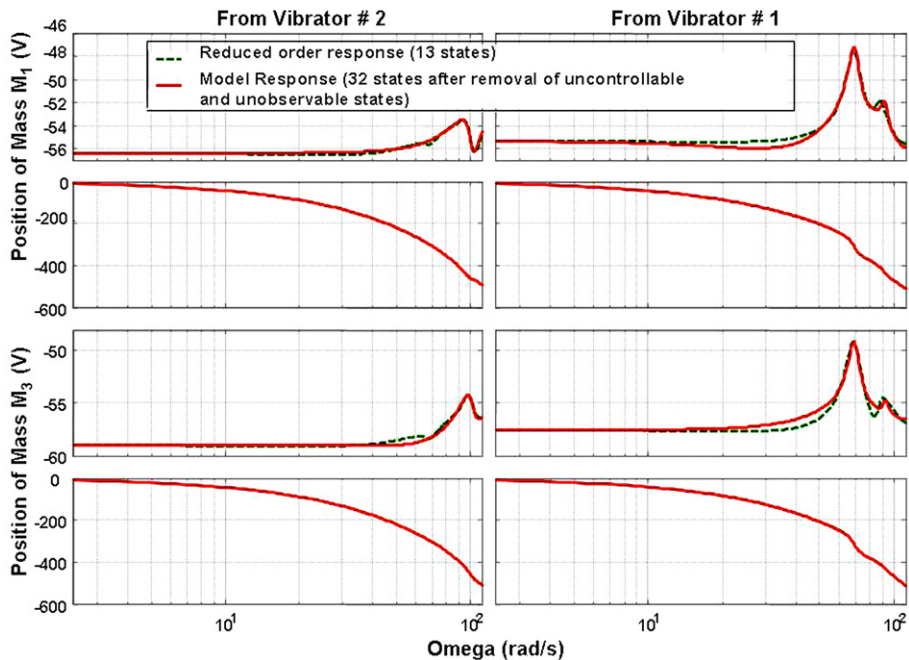


Fig. 4. Frequency response of full state and reduced order model.

By Castigliano’s theorem,

$$\begin{aligned}
 U &= \int_0^{L_4} \frac{M_0^2 dz}{2EI} = \frac{1}{2EI} \int_0^{L_4} F_1^2(L_5 - z)^2 dz, \\
 U &= \frac{1}{2EI} \int_0^{L_4} F_1^2(L_5^2 - 2L_5z + z^2) dz = \frac{F_1^2}{2EI} \left(L_4L_5^2 - L_5L_4^2 + \frac{L_4^3}{3} \right), \\
 \delta(\text{free}) &= \frac{\partial U}{\partial F_1} = \frac{F_1L_4}{EI} \left[L_5^2 - L_5L_4 + \frac{L_4^2}{3} \right], \\
 \Rightarrow k &= \frac{3EI}{L_4(3L_5^2 - 3L_5L_4 + L_4^2)}.
 \end{aligned}
 \tag{2}$$

Hence, the natural frequency is

$$\omega_n = \sqrt{\frac{k}{m_3}} = \sqrt{\frac{3EI}{m_3L_4(3L_5^2 - 3L_5L_4 + L_4^2)}}.
 \tag{3}$$

The forced single-input single-output (SISO) system equation in Fig. 3 is obtained as

$$m\ddot{z} + kz = F_1,
 \tag{4}$$

$$\dot{\mathbf{x}} = A\mathbf{x} + B\mathbf{u},$$

$$\mathbf{y} = C\mathbf{x} + D\mathbf{u},
 \tag{5}$$

where

$$\mathbf{x} = \begin{pmatrix} x \\ \dot{x} \end{pmatrix}; \quad A = \begin{pmatrix} 0 & 1 \\ -k/m_3 & 0 \end{pmatrix}; \quad B = \begin{pmatrix} 0 \\ 1 \end{pmatrix}; \quad C = (1 \quad 0); \quad D = (0); \quad \mathbf{y} = (x),$$

x and \dot{x} represent, respectively, the modal displacement of the mass m_3 from the center of the beam or the rest position and its velocity in the x -direction.

3.1.2. Analysis of System 2

For the 1-input 2-output System 2, m_2 is assumed to be a point mass located at the tip of Beam 2. The lateral displacements of beam 1 and 2, $y_i(x_i)$, $i = 1, 3$ are approximated by third order polynomials in x_i , $i = 1, 3$ and the lateral displacement of mass m_1 , $y_2(x_2)$, is approximated by a linear fit in x_2 as seen in Fig. 1

$$y_1(x_1) = C_1 \frac{x_1^3}{6} + C_2 \frac{x_1^2}{2} + C_3x_1 + C_4,$$

$$y_2(x_2) = C_5x_2 + C_6,$$

$$y_3(x_3) = C_7 \frac{x_3^3}{6} + C_8 \frac{x_3^2}{2} + C_9x_3 + C_{10}.$$

The above polynomial approximation is based on the assumption that mass m_1 is treated as a rigid body with negligible deformation, because of its dimensions and Young’s Modulus of the material and the forces that it experiences. With the definitions $\bar{y}_2(\frac{L_2}{2})$ and $\bar{y}_3(L_3)$, the boundary conditions at the end points and the compatibility conditions are given below in equation.

3.1.2.1. *Boundary conditions.* Beam 1 is modelled as a cantilever and hence both the displacement and velocity at the fixed end of the beam are zero

$$y_1(0) = 0; \quad y_1'(0) = 0.$$

Also, the cantilever beam is attached to a mass m_1 which in this case is modelled as a beam. Hence, by the continuity principle, the displacement at the interface of Beam 1 and mass m_1 should be the same.

$$y_1(L_1) = y_2(0); \quad y_1'(L_1) = y_2'(0).$$

Writing the flexural bending equation for Beam 1 with Young's modulus E_1 and the area moment of inertia I_1 :

$$E_1 I_1 y_1''(L_1) = M_B^+; \quad -E_1 I_1 y_1'''(L_1) = V_B^+,$$

where M_B is the bending moment at the interface of Beam 1 and mass m_1 and V_B is the shear force acting at the interface. Convention used is + sign for clockwise moment and shear force producing clockwise moment. The following equations are obtained from similar analysis and sign convention used for the interface between mass m_1 and Beam 2:

$$\begin{aligned} y_2(L_2) &= y_3(0); & y_2'(L_2) &= y_3'(0), \\ E_3 I_3 y_3''(0) &= M_C^-; & -E_3 I_3 y_3'''(0) &= V_C^-, \\ E_3 I_3 y_3''(L_3) &= 0; & E_3 I_3 y_3'''(L_3) &= m_2 \ddot{y}_3 - F_2, \end{aligned}$$

where E_3 is the Young's modulus and I_3 is the area moment of inertia of Beam 2. The last equation is derived with F_2 being the force applied by Shaker 2.

3.1.2.2. Compatibility conditions. Considering the equilibrium of each individual beam and mass in the single input, multi-output system, the following compatibility conditions are obtained:

$$\begin{aligned} \sum \text{Bending moments @ } B &= 0 \text{ (taking clockwise+)} \\ \Rightarrow -M_B^+ + M_C^- + V_C^- L_2 - m_1 \ddot{y}_2 \frac{L_2}{2} &= 0, \end{aligned} \tag{6}$$

$$\begin{aligned} \sum \text{Forces @ } B &= 0 \text{ (taking rightwards+)} \\ \Rightarrow -V_B^+ + V_C^- - m_1 \ddot{y}_2 &= 0, \end{aligned} \tag{7}$$

where E_i represents the Young's modulus of the beam and I_i represents the area moment of inertia of the Beam i . Also, M_C and V_C represent the bending moment and shear force at the interface of mass m_1 and Beam 2. Applying these boundary and compatibility conditions and solving manually for all constants in terms of parameters of Young's modulus, the area moment of inertia, forces, lengths and masses, the following expressions for the 10 constants, C_1 to C_{10} are obtained in terms of measurable physical parameters.

$$\begin{aligned} C_1 &= -\frac{1}{E_1 I_1} [F_2 - m_2 \ddot{y}_3 - m_1 \ddot{y}_2], \\ C_2 &= \frac{(L_1 + L_2 + L_3)}{E_1 I_1} [F_2 - m_2 \ddot{y}_3] + \frac{(2L_1 + L_2)}{2E_1 I_1} [-m_1 \ddot{y}_2], \\ C_3 &= C_4 = 0, \\ C_5 &= \frac{(L_1^2 + 2L_1 L_2 + 2L_1 L_3)}{2E_1 I_1} [F_2 - m_2 \ddot{y}_3] + \frac{(L_1^2 + L_1 L_2)}{2E_1 I_1} [-m_1 \ddot{y}_2], \\ C_6 &= \frac{(2L_1^3 + 3L_1^2 L_2 + 3L_1^2 L_3)}{6E_1 I_1} [F_2 - m_2 \ddot{y}_3] + \frac{(4L_1^3 + 3L_1^2 L_2)}{12E_1 I_1} [-m_1 \ddot{y}_2], \\ C_7 &= -\frac{1}{E_3 I_3} [F_2 - m_2 \ddot{y}_3], \\ C_8 &= -\frac{L_3}{E_3 I_3} [F_2 - m_2 \ddot{y}_3], \\ C_9 &= C_5, \\ C_{10} &= \frac{(2L_1^3 + 6L_1^2 L_2 + 6L_2^2 L_1 + 3L_1^2 L_3 + 6L_1 L_2 L_3)}{6E_1 I_1} [F_2 - m_2 \ddot{y}_3] + \frac{(4L_1^3 + 9L_1^2 L_2 + 6L_1 L_2^2)}{12E_1 I_1} [-m_1 \ddot{y}_2]. \end{aligned}$$

Substitution of the constants in Eqs. (6) and (7) yields the following dynamic equations:

$$m_1 \ddot{\bar{y}}_2 + P\bar{y}_2 + Q\bar{y}_3 = 0$$

and

$$m_2 \ddot{\bar{y}}_3 + R\bar{y}_2 + S\bar{y}_3 = F_2.$$

The parameters $P, Q, R,$ and S are obtained from the following equations:

$$P = \frac{a_4}{a_1 a_4 - a_2 a_3},$$

$$Q = \frac{-a_2}{a_1 a_4 - a_2 a_3},$$

$$R = \frac{a_3}{a_3 a_2 - a_1 a_4},$$

$$S = \frac{-a_1}{a_3 a_2 - a_1 a_4},$$

where the constants a_1, a_2, a_3 and a_4 are determined as follows:

$$a_1 = \left[\frac{4L_1^3 + 6L_1^2 L_2 + 3L_1 L_2^2}{12E_1 I_1} \right],$$

$$a_2 = \left[\frac{4L_1^3 + 9L_1^2 L_2 + 6L_1 L_2^2 + 6L_1^2 L_3 + 6L_1 L_2 L_3}{12E_1 I_1} \right],$$

$$a_3 = \left[\frac{4L_1^3 + 9L_1^2 L_2 + 6L_1 L_2^2 + 6L_1^2 L_3 + 6L_1 L_2 L_3}{12E_1 I_1} \right],$$

$$a_4 = \left[\frac{L_1^3}{3E_1 I_1} + \frac{L_3^3}{3E_3 I_3} + \frac{L_1^2 L_2 + L_1 L_2^2 + L_1^2 L_3 + L_1 L_3^2 + 2L_1 L_2 L_3}{E_1 I_1} \right].$$

Conversion to the single-input multiple-output (SIMO) state space form yields

$$\dot{\mathbf{x}} = \mathbf{A}\mathbf{x} + \mathbf{B}\mathbf{u},$$

$$\mathbf{y} = \mathbf{C}\mathbf{x} + \mathbf{D}\mathbf{u}, \tag{8}$$

$$\mathbf{x} = \begin{pmatrix} \bar{y}_2 \\ \dot{\bar{y}}_2 \\ \bar{y}_3 \\ \dot{\bar{y}}_3 \end{pmatrix}; \quad \mathbf{A} = \begin{pmatrix} 0 & 1 & 0 & 0 \\ -P/m_1 & 0 & -Q/m_1 & 0 \\ 0 & 0 & 0 & 1 \\ -R/m_2 & 0 & -S/m_2 & 0 \end{pmatrix};$$

$$\mathbf{B} = \begin{pmatrix} 0 \\ 0 \\ 0 \\ 1/m_2 \end{pmatrix}; \quad \mathbf{C} = \begin{pmatrix} 1 & 0 & 0 & 0 \\ 0 & 0 & 1 & 0 \end{pmatrix}; \quad \mathbf{D} = \begin{pmatrix} 0 \\ 0 \end{pmatrix};$$

$$\mathbf{y} = \begin{pmatrix} \bar{y}_2 \\ \bar{y}_3 \end{pmatrix},$$

where $\bar{y}_2, \dot{\bar{y}}_2, \bar{y}_3$ and $\dot{\bar{y}}_3$ represent the displacements and velocities of mass m_1 and m_2 , respectively.

The above analysis reveals that the single mass-beam system has a resonant frequency at 73.3 rad/s corresponding to mass m_3 and the two mass-beam system has resonant frequencies at 28.9 rad/s and 87.8 rad/s, which approximately correspond to the masses m_2 and m_1 , respectively. The idea behind the design is to obtain the resonant frequency of System 1 and the higher mode frequencies of System 2 as close as possible to each other so as to facilitate uniform probabilities of failure in two of the three specimens. However, this may require the specimens to be identical for comparison of their fatigue damage behavior.

4. System identification

A set of open loop plant models is typically derived based on a priori information (e.g., fundamental laws of physics, plant operating conditions and physical dimensions). The plant model parameters can be identified via time-domain or frequency domain techniques.

4.1. Open loop frequency domain identification

Both the time-domain and frequency-domain approaches are expected to yield equivalent results [5], in general. However, since the mechanical system under consideration is highly resonant and we are interested in accurate assessment of the resonant frequencies in this paper, a frequency-domain method of system identification [6] has been adopted based on sinusoidal sweep input excitation. Furthermore, the instrumentation of the test apparatus allows acquisition of experimental data in the frequency domain.

Non-parametric frequency domain identification makes use of transfer function measurements via combination of a slowly swept sine with a tracking filter. The reason for choosing the sinusoidal sweep as an input signal is to capture the resonant peaks that are the modes of the system without any undesired loss of accuracy. In this case, the system is characterized by measurements of the frequency response at a large number of discrete frequency points within the spectrum. In contrast, the parametric model is characterized by a number of selected parameters.

4.2. Frequency response of plant dynamics

The frequency domain modelling requires the plant output response at a set of discrete frequency points $\omega_k \in \{\omega_1, \omega_2, \dots, \omega_N\}$ covering the bandwidth of interest (i.e., from 0 to 20 Hz). An application of curve fitting techniques [7] yields a rational transfer matrix to obtain a closed form autoregressive moving average (ARMA) model

$$H(z) = \frac{A_0 + A_1z^{-1} + A_2z^{-2} + \dots + A_mz^{-m}}{1 + b_1z^{-1} + b_2z^{-2} + \dots + b_nz^{-n}}, \quad (9)$$

where the coefficient b_0 is normalized to unity and A_i 's represent the $\ell \times p$ coefficient matrices of numerator polynomials; the number of inputs is p and the number of outputs is ℓ and the b_i 's are the coefficients of the common denominator polynomial of degree n .

System identification is accomplished by using the frequency response data via the *invfreqz* algorithm of the *freqid* GUI package [8] under MATLAB. A sweeping sinusoidal signal over discrete frequencies in the bandwidth of the actuator is applied and the resulting output is collected. Similar results could also be achieved by attaching a frequency analyzer to the system. This is done by individually applying an input excitation to each actuator successively and collecting the respective output. Figs. 5 and 6 present Bode plots of the actual experimental data with each single input multi-output (SIMO) experiment. The identification is conducted with a sampling time of 2 ms for the data acquisition. The frequency ω of the excitation signal ranges from 0 to 113.1 rad/s (approx 18 Hz) with 176 points. The procedure followed in model identification is to minimize the frequency-weighted cost functional of the deviation of the model response from the generated plant data.

Algorithm. By default, *invfreqz* uses the principle of least squares to identify the model from the data series. This is accomplished by determining the transfer function coefficients by minimizing a cost functional in the following form:

$$C(A_k, b_k) = \min \sum_{x=1}^n \sum_{y=1}^n \left(\frac{1}{2} \sum_{i=1}^N W_{xy,i} \left| H_{xy}(\omega_i) \left(\sum_{k=0}^n b_k z_i^{-k} - \sum_{k=0}^m A_{xy,k} z_i^{-k} \right) \right|^2 \right), \quad (10)$$

where $H_{xy}(\omega_i)$ is the actual experimental frequency response at ω_i and $W_{xy,i}$ is the weighting factor for each frequency point ω_i . The weights are chosen as the inverse of the data in order to minimize a relative error instead of the absolute error. Furthermore, since Eq. (10) is a sum of quadratic terms, the cost functional

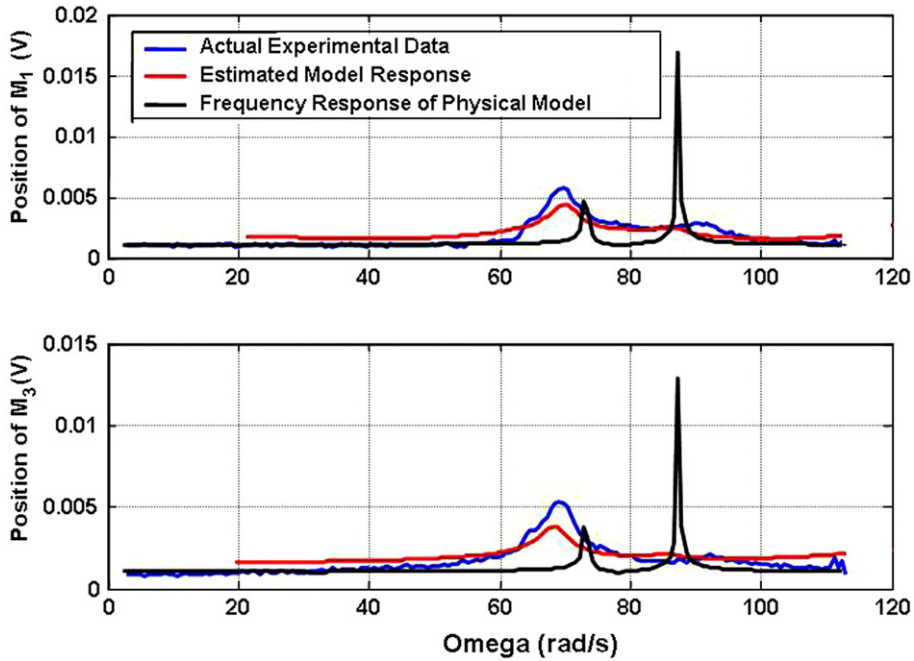


Fig. 5. Output positions vs input voltage to Shaker 1.

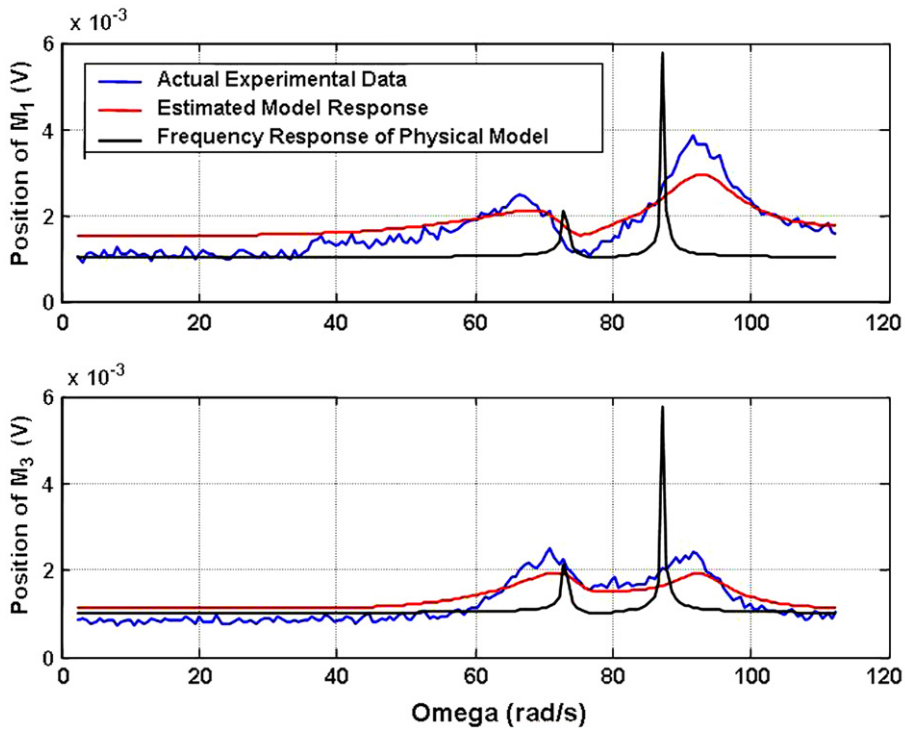


Fig. 6. Output positions vs input voltage to Shaker 2.

$C(A_k, b_k)$ can be minimized using numerical techniques (e.g., Newton–Gauss and Levenberg–Marquardt) for solving non-linear least-square problems. The analysis can be done in the complex field by ensuring that the coefficients A_k, b_k are real.

4.3. Data acquisition and estimation of transfer matrices

Output data are collected at steady state (i.e., allowing the transients to die out) over a sufficient length of time.

The results of the SIMO system experiments are presented in Figs. 5 and 6. Resonant frequencies are seen to be located at approximately 71 rad/s and 91 rad/s, which are very close to those predicted by the derived model.

Individual transfer functions are then identified for each input output pair and then the models are combined. Furthermore, the combined model is reduced to a minimal realization removing the uncontrollable and unobservable states using the *Staircase Algorithm*. The minimal realization is further balanced using the Matlab function *sysbal* to first isolate states with negligible contribution to the input/output response. While the order of state-space model was further reduced based on the magnitude of Hankel singular values [9] and by using the Matlab function *modred*, it was ensured that the resonant peaks (poles) of the original higher order model are conserved in the reduced order model having 13 states as shown in Fig. 4. This was done without any significant loss of information in the desired frequency range. Since, the system is highly resonant, the excess stable zeros were removed during model order reduction.

5. Experimental results and discussion

This section presents the results of the derived model and compares them with the experimental data. Figs. 5 and 6 exhibit comparison of the model responses with experimentally generated frequency response data (FRD) under excitation of Shaker #1 and Shaker #2, respectively. The model fairly captures the resonant peaks that correspond to the modes of the mechanical structure. Physical modelling of the system indicates the resonant peaks at 73.3 rad/s and 87.8 rad/s. The identified poles at 71 rad/s and 91 rad/s are close to the resonant peaks at 73.3 rad/s and 87.8 rad/s, obtained from the physical model (see Section 3.1). The small deviations in the resonant frequencies of the physical model from those obtained experimentally are possibly due to lumped parameter approximation and interactions between the two systems, which has not been incorporated in the physical model.

The transfer matrix of the open loop model of the test apparatus structure has been identified in the discrete-time setting with a sampling period of 0.002 s. The balanced and reduced model has 13 states, two control (i.e., actuator command) inputs, two outputs (i.e., displacement of the masses m_1 and m_3). Displacement of m_1 will be treated as the performance variable to synthesize the robust control law in the future. The discrete-time dynamic model of the plant with a sampling period $T_s = 0.002$ s is presented below:

$$x(k+1) = Ax(k) + Bu(k), \quad (11)$$

$$y(k) = Cx(k) + Du(k), \quad (12)$$

where

$$A = \begin{bmatrix} -0.8442 & 0.1770 & 0.1688 & 0.2314 & 0.0843 & 0.1274 & -0.0515 & 0.0142 & -0.0287 & 0.0356 & 0.0108 & 0.0019 & -0.0025 \\ -0.1790 & -0.1979 & 0.8040 & -0.2611 & -0.1083 & -0.1624 & 0.0581 & -0.0136 & 0.0366 & -0.0363 & -0.0141 & -0.0027 & 0.0062 \\ 0.1704 & -0.8047 & 0.1933 & 0.2670 & 0.1085 & 0.1629 & -0.0588 & 0.0143 & -0.0362 & 0.0372 & 0.0140 & 0.0027 & -0.0058 \\ -0.2246 & -0.2554 & -0.2622 & 0.6332 & -0.1934 & -0.3078 & 0.0742 & -0.0428 & 0.0544 & 0.0532 & -0.0274 & -0.0079 & 0.0052 \\ 0.0385 & 0.0448 & 0.0460 & 0.0763 & -0.8356 & 0.3686 & 0.1668 & 0.0598 & -0.1188 & -0.0238 & 0.0386 & 0.0074 & 0.0097 \\ -0.0641 & -0.0845 & -0.0859 & -0.1761 & -0.3685 & -0.0273 & -0.7588 & -0.2019 & 0.0985 & 0.0759 & -0.0487 & -0.0171 & -0.0570 \\ 0.0356 & 0.0519 & 0.0511 & 0.1132 & 0.0784 & 0.6154 & 0.1701 & -0.2355 & 0.4704 & -0.1464 & -0.0868 & -0.0010 & -0.0480 \\ -0.0672 & -0.0846 & -0.0850 & -0.1503 & -0.0186 & 0.0223 & 0.3442 & -0.7033 & -0.2474 & 0.3898 & -0.0305 & -0.0336 & 0.0546 \\ -0.0329 & -0.0330 & -0.0332 & -0.0201 & 0.1623 & 0.3410 & -0.2617 & -0.0133 & -0.5714 & -0.3410 & -0.0759 & -0.0407 & 0.1648 \\ 0.0379 & 0.0471 & 0.0479 & 0.0801 & 0.0299 & -0.0830 & -0.1877 & -0.4305 & 0.2346 & -0.2553 & 0.3867 & 0.1566 & 0.4556 \\ 0.0225 & 0.0264 & 0.0265 & 0.0342 & -0.0383 & -0.0831 & 0.0508 & -0.0751 & -0.2174 & -0.2434 & -0.3498 & 0.7174 & -0.0729 \\ -0.0024 & -0.0036 & -0.0035 & -0.0070 & -0.0013 & -0.0173 & -0.0117 & -0.0138 & 0.1281 & -0.0237 & -0.7711 & -0.2423 & 0.4656 \\ 0.0026 & 0.0012 & 0.0012 & -0.0097 & -0.0445 & -0.0810 & 0.0958 & -0.0464 & -0.1005 & -0.4619 & 0.0861 & -0.5648 & -0.0590 \end{bmatrix}$$

$$\begin{array}{r}
0.0169 \quad 0.0240 \\
-0.0172 \quad -0.0238 \\
0.0170 \quad 0.0239 \\
-0.0192 \quad -0.0226 \\
0.0129 \quad -0.0056 \\
-0.0127 \quad 0.0094 \\
B = -0.0145 \quad 0.0060 \\
0.0000 \quad -0.0008 \\
0.0020 \quad -0.0079 \\
0.0059 \quad -0.0027 \\
-0.0024 \quad 0.0036 \\
0.0017 \quad -0.0009 \\
-0.0019 \quad 0.0031 \\
C = \begin{array}{cccccccccccc}
-0.0249 & -0.0240 & -0.0239 & -0.0251 & 0.0004 & -0.0019 & 0.0038 & -0.0062 & -0.0013 & -0.0072 & 0.0002 & -0.0001 & -0.0035 \\
-0.0164 & -0.0180 & -0.0183 & -0.0178 & -0.0039 & 0.0021 & 0.0018 & 0.0114 & 0.0050 & 0.0062 & 0.0002 & 0.0009 & 0.0054 \\
1.0e-005^*
\end{array} \\
D = \begin{array}{cc}
0.2628 & -0.4518 \\
-0.1784 & 0.3757.
\end{array}
\end{array}$$

6. Detection of fatigue crack anomaly

The mechanical system in Fig. 1 has been persistently excited over a frequency range, including the resonance frequency, so as to induce a stress level that causes fatigue failure to yield an average life of approximately 20,000 cycles, equivalently, a total duration of about 32 min. The applied stress is dominantly flexural (i.e., bending) in nature and the amplitude of oscillations is symmetrical about the zero mean level. That is, the beams are subjected to reversed stress cycles [10]. Under such cyclic loading conditions, the specimens undergo fatigue cracking where the far-field stress is elastic and plasticity is only localized at the crack tip. The fatigue damage occurs at a time scale that is (several order of magnitude) slow relative to the fast time scale dynamics of the vibratory motion and eventually leads to a complete breakage of the beam structure at the failure site. Close observation indicates that fatigue failure develops in the following pattern:

- The repeated cyclic stress causes incremental crystallographic slip and formation of persistent slip bands;
- Gradual reduction of ductility in the strain-hardened areas results in the formation of submicroscopic cracks and
- The notch effect of the submicroscopic cracks concentrates stresses until complete fracture occurs.

Crack initiation may occur at a microscopic inclusion or at site(s) of local stress concentration. In this experimental apparatus, the sites of stress concentration are localized by creating a hole in each of the three specimens as shown in Fig. 2.

Since the mechanical structure of the test apparatus consists of beams and masses, the underlying dynamics can be approximated by a finite set of first order coupled differential equations with parameters of damping and stiffness. The damping coefficients are very small and the *stiffness* constants very slowly change due to the evolving fatigue crack.

The anomaly detection methodology as proposed by Ray [1] has been evaluated with time-series data generated from the test apparatus in Fig. 1. Both shaker tables were excited by a sinusoidal input of amplitude 0.85 V and frequency 11.39 Hz (71 rad/s) throughout the run of each experiment. The time series data of Mass #3 displacement sensor, which serve as an indicator of the macroscopic system performance, were collected from the beginning of the experiments until breakage of specimens. The ensemble of data were saved in

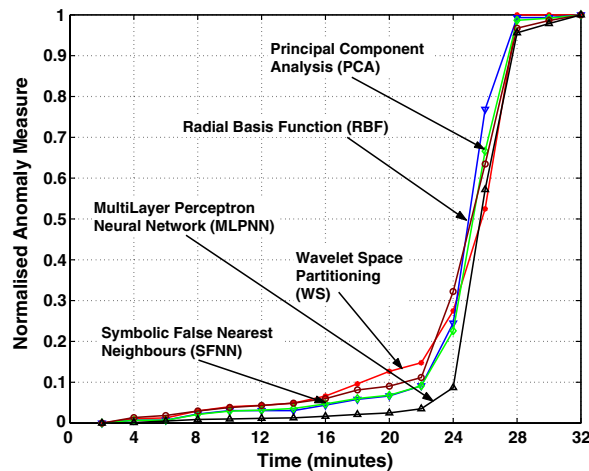


Fig. 7. Anomaly measure under persistent stimulus.

a total of 18 files, with each file containing 2 min of sensor time-series data. The time-series data sets were collected after the dynamic response attained the stationary behavior. The first data set was taken as the reference point representing the nominal behavior of the dynamical system. These data sets were used to compare the anomaly detection capability of the symbolic dynamics approach [1] relative to that of three established pattern recognition techniques: principal component analysis (PCA) [11], radial basis function neural network (RBFNN) [12] and multi-layer perceptron neural network (MLPNN) [13]. Some of the details are reported in [14].

The five plots in Fig. 7 compare the anomaly measures obtained by using five anomaly detection approaches, symbolic false nearest neighbors (SFNN) [15], wavelet space (WS) [1], PCA, MLPNN and RBFNN; details of the comparative analysis are reported in a previous publication [16]. The comparative analysis in this paper was performed for the first 16 files (i.e., up to 32 min when the service life of the test specimen is virtually expired, i.e., the specimen is about to break). *Note:* The estimated service life of the specimen under this load excitation is about 40 min, equivalently, the data contained in 20 files. The nominal condition is chosen at the time epoch of 2 min to ensure that all transients have decayed. The symbolic dynamics-based anomaly detection with both SFNN and WS partitioning yields the best performance and the MLPNN yields the worst performance in terms of early detection of anomalies. Both SFNN and WS are capable of detecting the anomaly within 16 min when the remaining life is more than 50% of the total service life of 32 min. In contrast, MLPNN is found to take more than 24 min to detect the anomaly at a similar level, which is equivalent to having the remaining life less than 20% of the total service life of 32 min. The distributed nonlinearities in the MLPNN may not be specifically suited to capture the small parameter perturbations in the largely linear behavior of the dynamic response of the vibrating structures. The WS-partitioning [1] with a proper choice of scales and mother wavelet shows significant higher anomaly measure as compared to PCA. The rationale is that the PCA method is dependent on eigenvalues and eigenvectors of the covariance matrix that is sensitive to measurement noise in the data acquisition process. In contrast, the symbolic dynamic approach, for both WS and SFNN partitioning, is much less sensitive to (zero-mean) measurement noise because of the inherent averaging due to repeated path traversing in the finite-state machine.

Test results show that the detection method is robust relative to modelling uncertainties within a few percent. Experimental data have been generated to quantify the statistical confidence levels on robustness as well as accuracy of the predicted remaining life based on anomaly measure. This is a topic of future research.

7. Conclusions and future work

This paper presents design, modelling and system identification of a laboratory test apparatus that has been constructed to experimentally validate the concepts of anomaly detection in complex mechanical systems. The

test apparatus is designed to be complex in itself due to partially correlated interactions amongst its individual components and functional modules. The experiments are conducted on the test apparatus to represent operations of mechanical systems where both dynamic performance and structural durability are critical.

The main objective of the work reported in this paper is design, modelling and system identification of an experimental apparatus to detect slowly evolving anomalies (e.g., decrease in stiffness due to fatigue failure) in complex mechanical systems at an early stage by observing time series data of the available displacement measuring sensors [14]. (Additional ultrasonic sensors will be installed at local crack sites in the future for enhancement of anomaly detection.) The information on evolving anomaly will serve as an input to the life extending control policy that will, in turn, generate corrective actions to mitigate fatigue crack damage in the specimen structures and thereby extend the remaining life of the specimens without any significant loss in performance [4]; synthesis and validation of the life extending control policy is a topic of future research. Nevertheless, the information on anomaly (i.e., fatigue crack damage) from the required time series data must be generated in *real time* by remote sensing if the failure site is not directly accessible to the measuring instruments that produce the time series data. Future work would involve usage of this real-time damage measure to synthesize control policies for mitigating failure and extending life without any significant loss in performance. A variety of sensor data (e.g., ultrasonic, acoustic emission, optical metrology, and displacement transducers) will be used to accurately assess the fatigue crack damage and predict the onset of widespread fatigue damage.

Further theoretical and experimental research is recommended in the following areas:

- Understanding deeper aspects of fatigue crack initiation using advanced sensing technology such as ultrasonics and electro-magnetics.
- Validation of the symbolic time series method for early detection of fatigue damage in different materials.
- Localization of crack incubation sites (possibly via acoustic emission) in large specimens.
- Formulation of decision and control policies for failure mitigation and life extension.
- Investigation of robustness of the detection method and accuracy of the predicted remaining life based on anomaly measure.
- Implementation of the anomaly detection methodology in *real-time* to facilitate life extension without any appreciable loss in performance.

Acknowledgments

The authors wish to thank Dr. Shin Chin for assistance in conducting neural network analysis in this research.

References

- [1] A. Ray, Symbolic dynamic analysis of complex systems for anomaly detection, *Signal Processing* 84 (7) (2004) 1115–1130.
- [2] H.D.I. Abarbanel, *The Analysis of Observed Chaotic Data*, Springer-Verlag, New York, 1996.
- [3] C.S. Daw, C.E.A. Finney, E.R. Tracy, A review of symbolic analysis of experimental data, *Review of Scientific Instruments* 74 (2) (2003) 915–930.
- [4] H. Zhang, A. Ray, S. Phoha, Hybrid life extending control of mechanical systems: experimental validation of the concept, *Automatica* 36 (1) (2000) 23–36.
- [5] R. Pintelon, J. Schoukens, Y. Rolain, Time domain identification, frequency domain identification. Equivalencies! differences? in: Tutorial Session-American Control Conference, July 2004.
- [6] L. Ljung, *System Identification: Theory for the User*, second ed., Prentice Hall, NJ, 1999.
- [7] E. Levi, Complex curve fitting, *IRE Transactions on Automatic Control* AC-4 (1959) 37–44.
- [8] R.A. de Callafon, Freqid: a gui for frequency domain identification. Available from: <<http://www.dcsc.tudelft.nl/Research/Software/index.html>>.
- [9] R.S. Sanchez-Pena, M. Szaier, *Robust Systems: Theory and Applications*, John Wiley, New York, NY, 1998.
- [10] M. Klesnil, P. Lukas, *Fatigue of metallic materials* Material Science Monographs, vol. 71, Elsevier, 1992.
- [11] R. Duda, P. Hart, D. Stork, *Pattern Classification*, John Wiley & Sons Inc., 2001.
- [12] C.M. Bishop, *Neural Networks for Pattern Recognition*, Oxford University Press Inc., New York, 1995.
- [13] S. Haykin, *Neural Networks: A Comprehensive Foundation*, Prentice Hall, Upper Saddle River, NJ, 1999.

- [14] A. Khatkhate, A. Ray, V. Rajagopalan, S. Chin, E. Keller, Detection of fatigue crack anomaly: a symbolic dynamics approach, in: Proceedings of American Control Conference, Boston, MA, 2004.
- [15] M.B. Kennel, M. Buhl, Estimating good discrete partitions from observed data: symbolic false nearest neighbors, 2003. Available from: <http://arxiv.org/PS_cache/nlin/pdf/0304/0304054.pdf>.
- [16] S. Chin, A. Ray, V. Rajagopalan, Symbolic time series analysis for anomaly detection: a comparative evaluation, *Signal Processing* 85 (9) (2005) 1859–1868.